Diabatic Heating Profiles in Recent Global Reanalyses

JIAN LING AND CHIDONG ZHANG

Rosenstiel School of Marine and Atmospheric Science, University of Miami, Miami, Florida

(Manuscript received 28 June 2012, in final form 15 October 2012)

ABSTRACT

Diabatic heating profiles are extremely important to the atmospheric circulation in the tropics and therefore to the earth's energy and hydrological cycles. However, their global structures are poorly known because of limited information from in situ observations. Some modern global reanalyses provide the temperature tendency from the physical processes. Their proper applications require an assessment of their accuracy and uncertainties. In this study, diabatic heating profiles from three recent global reanalyses [ECMWF Interim Re-Analysis (ERA-Interim), Climate Forecast System Reanalysis (CFSR), and Modern Era Retrospective Analysis for Research and Applications (MERRA)] are compared to those derived from currently available sounding observations in the tropics and to each other in the absence of the observations. Diabatic heating profiles produced by the reanalyses match well with those based on sounding observations only at some locations. The three reanalyses agree with each other better in the extratropics, where large-scale condensation dominates the precipitation process in data assimilation models, than in the tropics, where cumulus parameterization dominates. In the tropics, they only agree with each other in gross features, such as the contrast between the ITCZs over different oceans. Their largest disagreement is the number and level of heating peaks in the tropics. They may produce a single, double, or triple heating peak at a given location. It is argued that cumulus parameterization cannot be the sole source of the disagreement. Implications of such disagreement are discussed.

1. Introduction

Diabatic heating in the atmosphere is a combined consequence of radiative fluxes, phase changes of water substance, and turbulence flux of sensible heat from the earth's surface. In the tropics, it is the major driving force of the atmospheric circulation. Through that, it acts as a unique cross-scale link between cloud microphysics and the global energy and water cycles.

The importance of the vertical structure of diabatic heating cannot be overstated. The tropical atmospheric circulation does not respond directly to vertically integrated heating, which approximately corresponds to total surface precipitation in convective regions. It responds to the vertical gradient of diabatic heating. Upper-level stratiform heating is essential to the mean tropical large-scale zonal circulation (Hartmann et al. 1984; Houze 1997; Schumacher et al. 2004) and its variability (Cho and Pendlebury 1997; Mapes 2000). Large-scale moisture convergence in the boundary layer and lower troposphere as a main energy supply for the Madden–Julian oscillation (MJO; Madden and Julian 1971, 1972) is closely related to low-level heating (Wu 2003; Li et al. 2009). Unrealistic diabatic heating profiles may lead to systematic biases in global climate models (Zermeno and Zhang 2012, manuscript submitted to *J. Climate*).

Our knowledge on vertical structures of tropical diabatic heating is, however, limited for several reasons. Vertical structures of diabatic heating in numerical models are mainly determined by cumulus parameterization, which is often considered a source of model inability, especially tropical rainfall (e.g., Hirota et al. 2011). Their realism must be assessed against observations. Direct observational measurement of diabatic heating profiles is difficult. Vertical profiles of diabatic heating is often estimated as a residual of the heat budget (commonly known as the apparent heat source or Q1) using data collected from a synoptic-scale sounding array, a technique developed by Yanai et al. (1973) and practiced by many (e.g., Lin and Johnson 1996; Zhang and Lin 1997). Vertical profiles of mesoscale diabatic heating can be estimated from observations of aircraft radars (Mapes

Corresponding author address: Dr. Jian Ling, RSMAS/MPO, University of Miami, 4600 Rickenbacker Causeway, Miami, FL 33149.
E-mail: jling@rsmas.miami.edu

DOI: 10.1175/JCLI-D-12-00384.1

and Houze 1995) or ground radars (Mather et al. 2007; Schumacher et al. 2008). Deployment of sounding arrays, aircraft, and ground radars are very expensive and logistically challenging in the tropics. The availability of tropical diabatic heating profiles based on observations is limited to few field campaigns over specific locations during specific periods. They were scattered over the past half century, each practically representing a point in the global domain and covering periods from weeks up to 4 months (see section 2). They are indispensably useful in many ways but do not provide a global perspective of long-term means and variability of vertical structures of diabatic heating.

Diabatic heating profiles with global tropical coverage have been estimated from satellite retrievals (e.g., L'Ecuyer and Stephens 2003; Shige et al. 2004; Tao et al. 2006). Differences among retrieval algorithms, however, lead to large discrepancies in their vertical structures (Hagos et al. 2010; Ling and Zhang 2011). Further improvement is needed before they can be used in place of sounding-based heating profiles.

Global diabatic heating (Q1) profiles can be derived from global data assimilation products, commonly known as global reanalyses, using the Yanai et al. (1973) method (e.g., Nigam et al. 2000; Hagos et al. 2010). One of the most exciting features in some recent global reanalyses is their direct output of total temperature tendency term from physical processes (QT[1]; see section 2a). Diabatic heating from the reanalyses is, however, a by-product of data assimilation. It is not directly constrained by observed heating profiles. Instead, they are produced by parameterization schemes (primarily for precipitation, cloud, radiation, and boundary layer processes including surface fluxes) in data assimilation models constrained mainly by observed winds, temperature, and humidity. They are, therefore, directly subject to infection of all known and unknown maladies in parameterization schemes. Blindly using diabatic heating output from the reanalyses as observed truth in diagnostics for understanding and validation of numerical simulations would be a serious mistake. Meanwhile, with observational constraints in dynamic and thermodynamic fields (an advantage over numerical simulations), diabatic heating output from the reanalyses serves as a unique and independent source of information with the advantage of global and long-term coverage. A systematic evaluation of diabatic heating profiles from the reanalyses is needed for their appropriate applications. This is the motivation of the current study.

Diabatic heating from reanalyses can be evaluated for its three aspects: horizontal distributions, amplitudes, and vertical structures. Nigam et al. (2000) and Chan and Nigam (2009) have examined the first two to a certain extent. Hagos et al. (2010) compared heating profiles from selected reanalyses, satellite retrievals, and limited sounding observations. This current study continue the effort of Hagos et al. (2010) to evaluate the vertical structures of diabatic heating in three recent global reanalysis products: the European Centre for Medium-Range Weather Forecasts (ECMWF) Interim Re-Analysis (ERA-Interim; Dee et al. 2011), the Climate Forecast System Reanalyses (CFSR; Saha et al. 2010) from the National Centers for Environmental Prediction, and the Modern Era Retrospective Analysis for Research and Applications (MERRA; Rienecker et al. 2011) from the National Aeronautics and Space Administration (NASA). Their descriptions are given in section 2a.

Time-mean horizontal distributions of vertically integrated diabatic heating from the three reanalyses resemble that of precipitation estimated from satellite, especially over the oceans (Fig. 1). The main climate features are all reproduced by the reanalyses: the intertropical convergence zones (ITCZs), the southern Pacific convergence zone (SPCZ), the southern Atlantic convergence zone (SACZ), and the northern Pacific and Atlantic storm tracks. There are obvious discrepancies between the different products, especially over land (e.g., Africa, South America, Southeast Asia). They are not the concern of this study. The focus of this study is vertical structures of diabatic heating produced by the reanalyses. We will in this study (i) assess their realism, (ii) document their agreement and disagreement among themselves, and (iii) evaluate the potential implications of their disagreement. The first item can be attempted only to a limited extent by comparing diabatic heating profiles from the reanalyses to those based on sounding observations. The second item is achieved by comparing the time mean and seasonal cycle of diabatic heating from different reanalyses at selected locations (e.g., the ITCZ and storm tracks). The third item is discussed based on our knowledge of the role played by diabatic heating profiles in the climate system. We will also examine the extent to which Q1 (estimated as a heat budget residual using reanalysis wind and temperature data) can be used as a reliable proxy of QT (total diabatic heating as a temperature tendency term directly from the reanalysis output).

Data and methods are described in section 2. Results are presented in section 3. A summary and discussion are given in section 4.

[1] In this study, QT is used to refer to total diabatic heating output directly from reanalyses as temperature tendency due to all diabatic processes, as opposed to Q1, which is used to refer to total diabatic heating estimated as a residual of the thermodynamic equation.

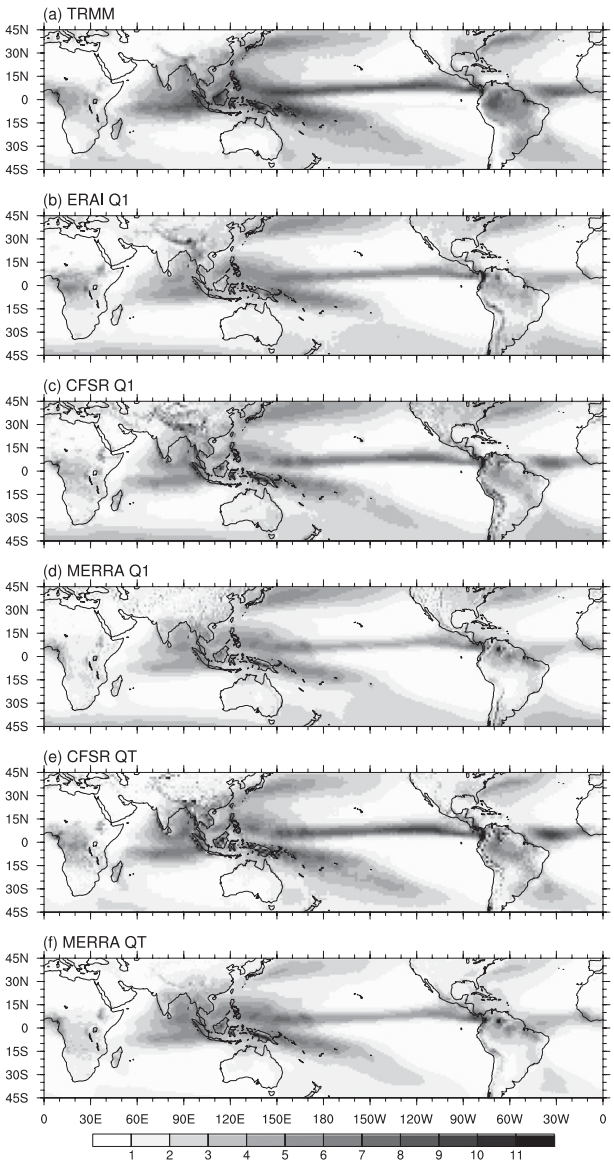

FIG. 1. Time-mean (a) precipitation (mm day^{-1}) from TRMM 3B42 (see section 2c) and mean vertically integrated heating (mm day^{-1}) from (b) ERA-Interim Q1, (c) CFSR Q1, (d) MERRA Q1, (e) CFSR QT, and (f) MERRA QT. All are averaged from 1980 to 2009.

2. Data and method

a. Reanalyses

Three global reanalyses (Table 1) were use in this study. The CFSR is the only global product by a coupled atmosphere–ocean–land surface–sea ice data assimilation system. The horizontal resolution is T382 (38 km) in its atmospheric component and about 0.5° in its oceanic component. There are 64 hybrid vertical layers in the atmosphere and 40 vertical layers in the ocean. The ERA-Interim is the part of preparation for the next generation extended reanalysis to replace the 40-yr ECMWF Re-Analysis (ERA-40). A four-dimensional variational data assimilation system (Rabier et al. 2000) is used in the Integrated Forecast System, a spectral model, with a horizontal resolution of T255 (80 km) and 60 hybrid vertical layers. MERRA is a product of the Global Modeling and Assimilation Office of NASA based on the Goddard Earth Observing System, version 5 (GEOS-5), data assimilation system with a horizontal resolution of ⅔° longitude by ½° latitude (55 km) with 72 Lagrangian vertical layers.

In this study, 30 yr (1980–2009) of data from the three reanalyses were used. CFSR and MERRA include direct output of temperature tendency terms related to diabatic processes; ERA-Interim does not. The direct output temperature tendency terms of all physics processes from CFSR and MERRA are regarded as total diabatic heating (QT). In addition, total diabatic heating (Q1; see section 2d) was estimated using gridpoint wind and temperature from all reanalyses following the method of Yanai et al. (1973) so they all can be compared directly with each other and with sounding-based Q1 estimates.

b. Sounding data

Apparent heating sources (Q1) estimated using wind and temperature from sounding observations of eight field campaigns (Table 2) were compared to Q1/QT from the reanalyses. These field campaigns took place in three general climate regimes. The first is the open ocean with only small or no islands, where the Tropical Ocean Global Atmosphere Coupled Ocean–Atmosphere Response Experiment (TOGA COARE), the Kwajelin Experiment (KWAJEX), and the *Mirai* Indian Ocean Cruise for the Study of the MJO Convection Onset (MISMO) took place. The second is the coastal and monsoon regions, where the South China Sea Monsoon Experiment's Northern and Southern Enhanced Arrays (SCSMEX N and SCSMEX S), Tropical Warm Pool International Cloud Experiment (TWP-ICE), and the North American Monsoon Experiment (NAME) were conducted. The Large-Scale Biosphere–Atmosphere Experiment in Amazonia (LBA) was in a unique continental rain forest region. The locations, durations, and references of these field campaigns are listed in Table 2. A detailed diagnostic of Q1 profiles based on these soundings was performed by Zhang and Hagos (2009).

c. Rainfall data

Daily rainfall data from the Tropical Rainfall Measuring Mission (TRMM; Kummerow et al. 2000) Multisatellite Precipitation Analysis (Huffman et al. 2007)

TABLE 1. Heating products from the reanalyses.

Name	References	Data type	Horizontal resolution	Tot vertical levels (1000–100 hPa)
ERA-Interim	Dee et al. 2011	Q1	1.5° lat × 1.5° lon	27
CFSR	Saha et al. 2010	QT, Q1	1.5° lat × 1.5° lon*	27
MERRA	Rienecker et al. 2011	QT, Q1	1.25° lat × 1.25° lon	25

* Regridded from original 0.5° latitude × 0.5° longitude.

were used in Fig. 1 to compare to horizontal distributions of vertical integrated Q1 and QT from the reanalyses. The horizontal resolution of the TRMM rainfall data is 0.25° × 0.25° and the coverage is 1998–2009.

Rainfall data are not available at all sounding locations. In place of rain rate, vertically integrated Q1 or QT (VIQ) is used,

$$\mathrm{VIQ} = \frac{c_p}{gL_c\rho_l}\sum_{i=1}^{n}\Delta p_i H_i, \tag{1}$$

where n is the number of vertical levels from 900 to 200 hPa, i is the index for vertical levels, Δp_i is the pressure layer depth, H_i is the diabatic heating rate at level i, L_c is latent heat of condensation at 0°C, c_p is the specific heat capacity of dry air, and ρ_l is the density of liquid water. The unit of VIQ is millimeters per day. The integration starts from 900 hPa to avoid sensible heating flux from the surface. Positive VIQ is a reasonable approximation of the rain rate under the assumption that when it rains latent heating dominates. Negative VIQ indicates column cooling, mostly due to longwave radiation.

d. Q1 estimates

Estimating total diabatic heating as the apparent heat source (Q1) using the daily reanalyses data and the approach of Yanai et al. (1973) has been practiced previously (Nigam et al. 2000; Zhou and Chan 2005; Hagos et al. 2010). Q1 is the residual of the thermodynamic equation,

$$\mathrm{Q1} = \frac{T}{\theta}\left(\frac{\partial\theta}{\partial t} + u\frac{\partial\theta}{\partial x} + v\frac{\partial\theta}{\partial y} + \omega\frac{\partial\theta}{\partial p}\right), \tag{2}$$

where u, v, and ω are the three-dimensional wind components and $\theta = T(p_{00}/p)^{R/c_p}$ is the potential temperature, with T being temperature, p being pressure and p_{00} being surface pressure (usually 1000 hPa), and R being the specific gas constant of dry air. Q1 was calculated from the three reanalyses at each grid using the four nearest grids. The extent to which Q1 is a good approximation of QT will be discussed.

3. Results

a. Comparison to sounding observations

The realism for diabatic heating (Q1 and QT) profiles from the reanalyses are assessed by comparing them to limited sounding observations from the field campaigns (Table 2). For each field campaign, a grid domain was defined to cover the sounding array (Table 2). Reanalysis Q1 and QT were averaged over the domain for the comparison to sounding-based Q1. Large discrepancies between their mean profiles exist partially because of their corresponding total amount of precipitation (approximated by VIQ). To emphasize their vertical structures in this comparison, each mean heating profile was normalized by its VIQ. The normalized diabatic heating profiles (K mm^{-1}) are shown in Fig. 2. Those from the reanalyses match well the observed at certain locations, such as MISMO and TOGA COARE, but not at others. The reanalyses all overestimate upper-level

TABLE 2. Sounding observations from field campaigns. The longitudes and latitudes specify the grid domains that cover the sounding arrays, over which reanalysis diabatic heating was averaged for the comparisons to sounding-based heating profiles.

Name	Lat	Lon	Duration*	Reference
MISMO	0°–3°N	73°–79°E	31 Oct–26 Nov 2006	Yoneyama et al. 2008
SCSMEX S	1.5°–8°N	105°–110°E	5 May–20 Jun 1998	Ding et al. 2004
SCSMEX N	18°–22°N	113°–120°E	5 May–20 Jun 1998	Ding et al. 2004
TOGA COARE	4°S–0°	152°–157°E	1 Nov 1992–28 Feb 1993	Webster and Lukas 1992
KWAJEX	7°–9.5°N	166°–169°E	24 Jul–14 Sep 1999	Yuter et al. 2005
TWP-ICE	13.5°–11°S	129.5°–132°E	19 Jan–12 Feb 2006	May et al. 2008
NAME	23°–29°N	108°–102°W	7 Jul–15 Aug 2004	Higgins et al. 2006
LBA	12°–9°S	64°–60°W	1 Nov 1998–28 Feb 1999	Silva Dias et al. 2002

* Used this this study.

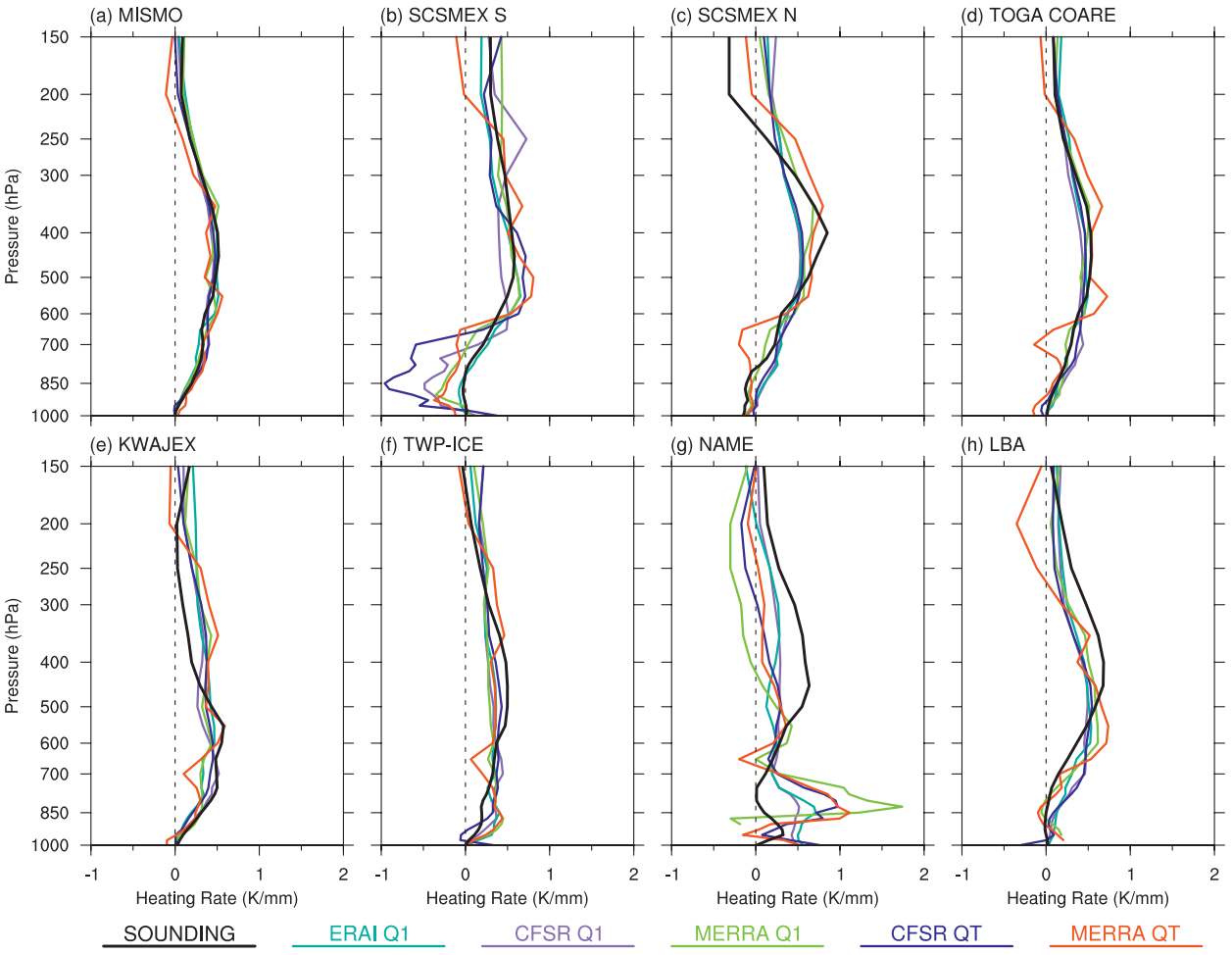

FIG. 2. (a)–(h) Normalized mean diabatic heating profiles (K mm^{-1}) from sounding observations and reanalyses at the eight field campaign locations listed in Table 2.

heating at KWAJEX, overestimate lower-level heating and underestimate upper-level heating at NAME and LBA, and overestimate lower-level cooling at SCSMEX S. It is unknown to what degree assimilating the field sounding observations into the reanalyses may play a role here. It is interesting that QT from MERRA shows a local minimum at 700 hPa at most locations, which has been pointed out by Ling and Zhang (2011) in their study on the MJO heating profiles during the TOGA COARE period.

In addition to the means, daily diabatic heating profiles from the reanalyses and sounding observations were also compared. Their daily correlation was calculated at each location. The days with their correlation at the 95% significant level were counted. The ratio of these days to the total number of the days (e.g., the percentage of days with significant correlation) at each location represents the degree to which overall daily profiles from the reanalyses and sounding observations match each other (Fig. 3a). This ratio ranges from 0.1 or 10% (CFSR and MERRA QT at NAME) to 0.75 or 75% (ERA-Interim Q1 at TWP-ICE). In most cases, it is between 0.4 and 0.7. There might be many factors determining why 30%–60% of the individual heating profiles from the reanalyses do not match the observed, such as the timing and exact locations of convective events. When this ratio is calculated using only the days when sounding VIQ is larger than 2 mm day^{-1}, its values increase in most cases[2] (Fig. 3b). This indicates that the reanalyses are more able to reproduce observed diabatic heating profiles during heavier than lighter precipitation periods. One exception is NAME, where the ratio becomes smaller for days of VIQ $>$ 2 mm day^{-1}. The reason for this might be that the NAME sounding array covered an area over the Gulf of California with both water and

[2] Results are not sensitive to this threshold.

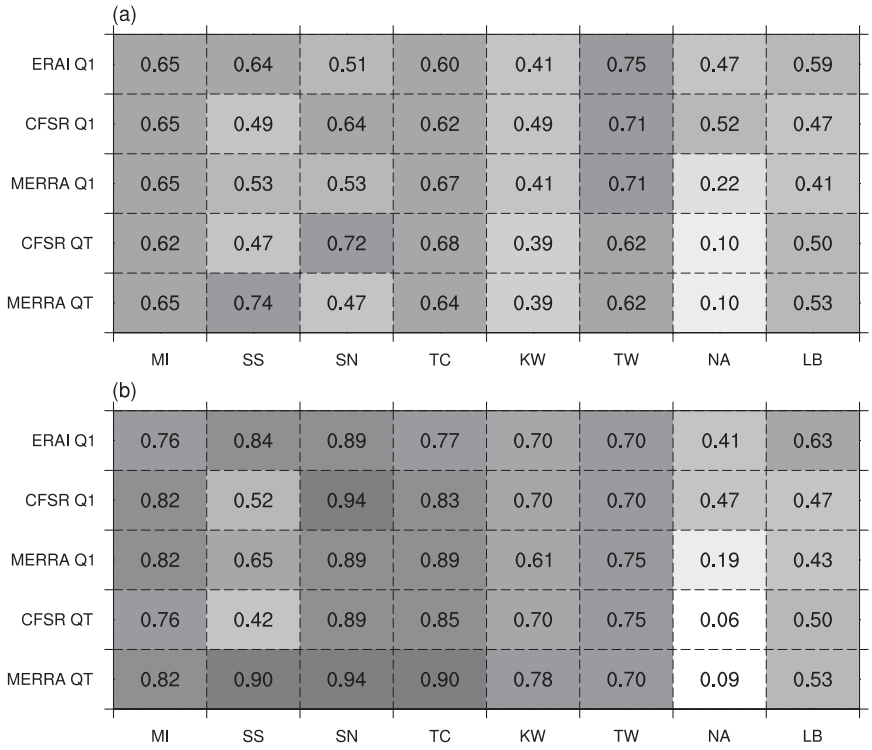

FIG. 3. (a) Percentage of the days with diabatic heating profiles of the reanalysis and sounding observations correlated at the 95% significance level at MISMO (MI), SCSMEX S (SS), SCSMEX N (SN), TOGA COARE (TO), KWAJEX (KW), TWP-ICE (TW), NAME (NA), and LBA (LB). (b) As in (a), but for VIQ $>$ 2 mm day^{-1}. Ratios between 0.3 and 0.6 are highlighted by light shading, and those larger than 0.6 are denoted by dark shading.

complex terrain (Higgins et al. 2006), which may not be well resolved by the reanalysis models. It also appears in Fig. 3b that heating profiles from the reanalyses are in a better agreement with the observed over the oceans than over land or coastal regions (SS, NA, and LB).

The general dependence of daily heating profiles on the rain rate (approximated by VIQ) for the reanalyses and sounding observations are compared in Fig. 4 using heating profiles at all eight sounding locations in combination. The peak of heating from sounding Q1 (Fig. 4d) is at 500–400 hPa for VIQ $>$ 0. Heating peak in ERA-Interim is slightly lower, near 600 hPa at light rain rates (VIQ $<$ 6 mm day^{-1}), and is elevated slightly at larger rain rates and rapidly at very high rain rates ($>$15 mm day^{-1}) (Fig. 4a). CFSR Q1 (Fig. 4b) shows larger discrepancies from sounding Q1. Its peak is near 700 hPa at light rain rates ($<$5 mm day^{-1}), but it shows double peaks for larger rain rates except for the very high ones ($>$12 mm day^{-1}). The double peaks are less obvious in CFSR QT (Fig. 4e) but are the most evident in MERRA Q1 and QT, which has been seen by Hagos et al. (2010). There is even a third peak in the boundary layer in MERRA QT (Fig. 4f). The lack of such multiple peaks in sounding Q1 forms a stark contrast to MERRA QT.

Several points should be made clear from the comparisons of the diabatic heating profiles of the reanalyses and sounding observations. First, the realism of reanalyses heating profiles varies with locations. The limited observational validation in Figs. 2 and 3 does not suggest how realistic heating profiles from the reanalyses might be at other locations. The realism of reanalyses heating profiles is very different at TOGA COARE and KWEJEX, with both being in the western Pacific warm pool environment. The accuracy of vertical heating profiles from the reanalyses at a given location cannot be assumed until they are validated directly against observations. Second, this limited comparison to observations does not tell which reanalyses may produce overall more realistic vertical heating profiles than the others. Correlation coefficients between the five reanalysis Q1 and QT products and sounding Q1 from all the eight locations combined are very close to each other (0.49–0.56). Third, consistency (small disagreement) among the reanalyses heating profiles does not mean a lack of biases. The biases at KWAJEX exemplify this. Fourth, as

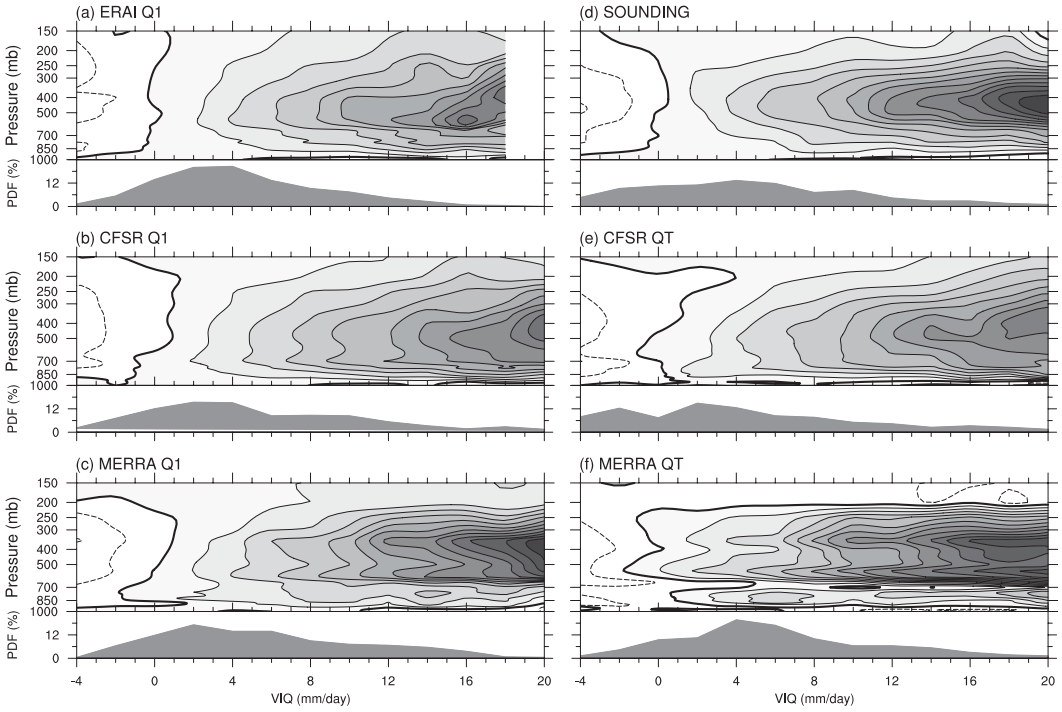

FIG. 4. Diabatic heating profiles (interval 1 K day^{-1}) as functions of (top) VIQ and (bottom) PDFs of VIQ (%) from (a) ERA-Interim Q1, (b) CFSR Q1, (c) MERRA Q1, (d) sounding Q1, (e) CFSR QT, and (f) MERRA QT for all eight field campaign locations in combination. The VIQ bin width is 2 mm day^{-1}. Dashed contours are for negative values, bold contours are for zeros, and positive values are highlighted by shading.

pointed out earlier, observed diabatic heating profiles over the ocean are generally better reproduced by the reanalyses than over land, especially with complicated topographic and surface conditions (e.g., NAME).

b. Zonal means

The limited sounding Q1 data are insufficient for a global assessment of the quality of heating profiles from the reanalyses. Similarities and differences among the reanalyses need to be explored. Even though they do not necessarily indicate the quality of the reanalysis heating products, their differences provide an envelope of uncertainties that must be known for their proper applications. Zonal-mean diabatic heating profiles from the reanalyses and its components over the oceans and land are compared in this subsection. Their overall meridional distributions are similar to each other (Fig. 5, left). Strong, deep tropical heating centers are flanked by deep tropospheric cooling in the subtropics (20°S and 20°N); boundary layer heating extending from the tropics to the extratropics in both hemispheres. This structure is consistent with the Hadley circulation. The strongest subtropical cooling is immediately above the boundary layer. A second but much weaker cooling peak is in the upper troposphere. There is a heating center at around 50° latitude and near 700–400 hPa in each hemisphere. Both tilt downward toward higher latitudes. As will be explained, the precipitation types in these two extratropical heating centers are different from those in the tropic heating center. In the tropics, all reanalyses heating exhibits multiple peaks. However, the levels of the peaks are very different. There are three peaks in MERRA Q1 (Fig. 5g) and QT (Fig. 5m), whereas the other heating products show one or two peaks. This disagreement among the reanalysis heating profiles will be discussed many times later in this study. Some reanalyses show distinct double ITCZ (CFSR Q1 in Fig. 5d and QT in Fig. 5j), others do not (ERA-Interim; Fig. 5a). For CFSR and MERRA, QT is generally stronger than Q1 in both heating and cooling. Their general spatial patterns are very similar.

These similarities and differences among the reanalysis heating profiles remain for the zonal means over the ocean only (Fig. 5, middle). Tropical heating over the ocean, coming mainly from the ITCZ, is slightly north of the equator. The repeating low-level subtropical cooling suggests it takes place mainly over the marine stratus regions. The cooling amplitudes differ considerably among the reanalyses. The difference may come from the cloud and radiation schemes used in the assimilation models.

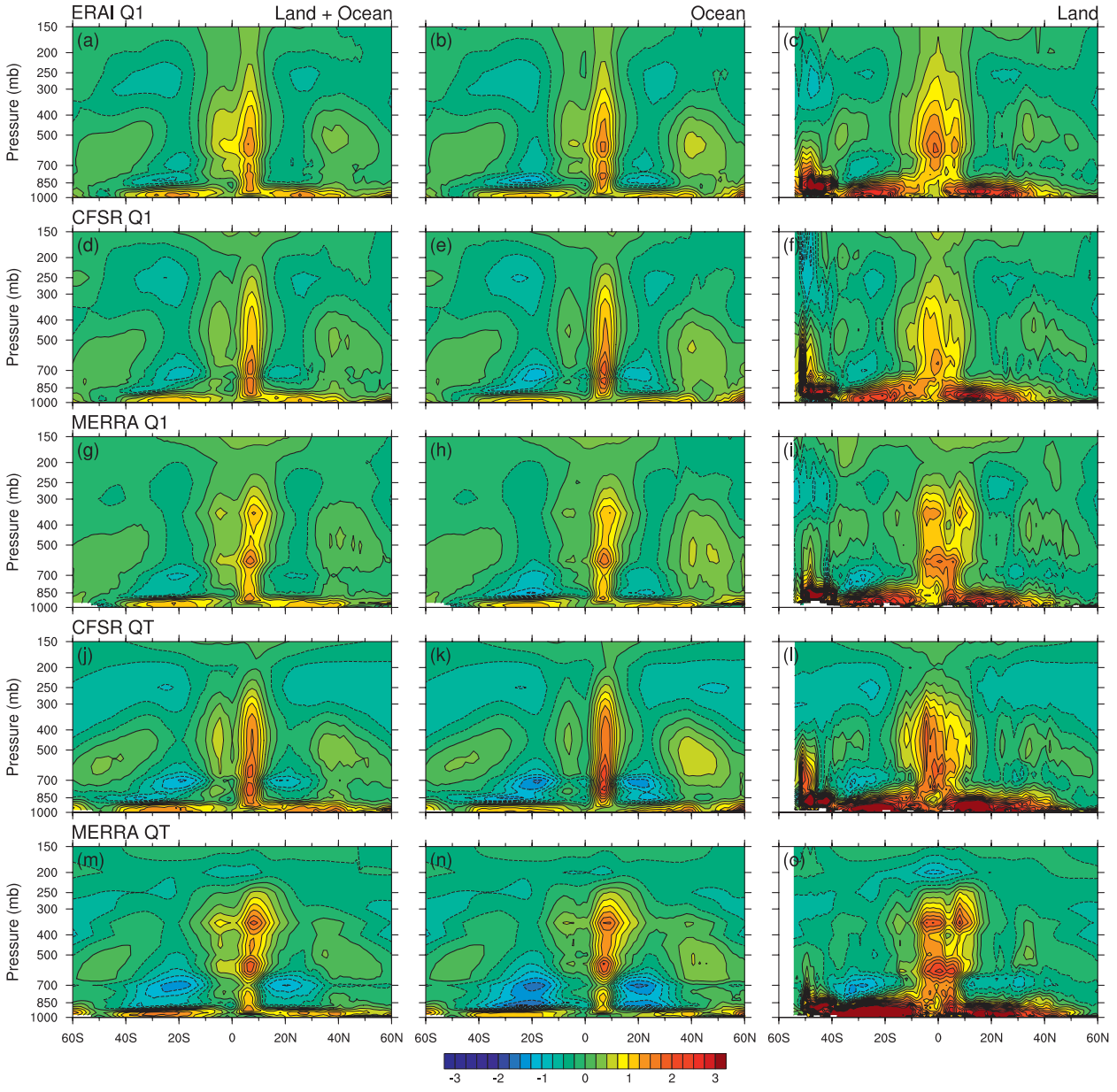

FIG. 5. Time and zonal means of diabatic heating (k day^{-1}) from (a)–(c) ERA-Interim Q1, (d)–(f) CFSR Q1, (g)–(i) MERRA Q1, (j)–(l) CFSR QT, and (m)–(o) MERRA QT for (left) total, (middle) over the oceans and (right) over land only.

There are two peaks in the low-level cooling in MERRA QT and, to a lesser degree, in CFSR QT. Zonal-mean heating profiles over land, in contrast, exhibits different characteristics. The tropical heating over land is much wider than over the oceans, signifying the contrast between rainfall of the monsoons and ITCZ. There are two tropical heating centers in some reanalyses (ERA-Interim in Fig. 5c; MERRA in Figs. 5i,o). The Southern Hemispheric heating is stronger than its Northern Hemispheric counterpart. This is due to stronger convection over land (the Amazon and Africa) during austral summer than boreal summer (over Central America, Africa, and Southeast Asia). The boundary heating is much stronger and deeper than over the ocean as expected because of strong sensible heat flux related to land surface heating. The extratropical tropospheric heating is weaker than over the oceans. The double heating peaks over the tropical oceans disappear over land in ERA-Interim (Fig. 5c) and CFSR (Figs. 5f,l). The three peaks in MERRA remain. There is a distinct strong lower-tropospheric heating center near 40°–50°S in all reanalyses over land, which is generated to the heavy rainfall on the west mountainside of the Andes.

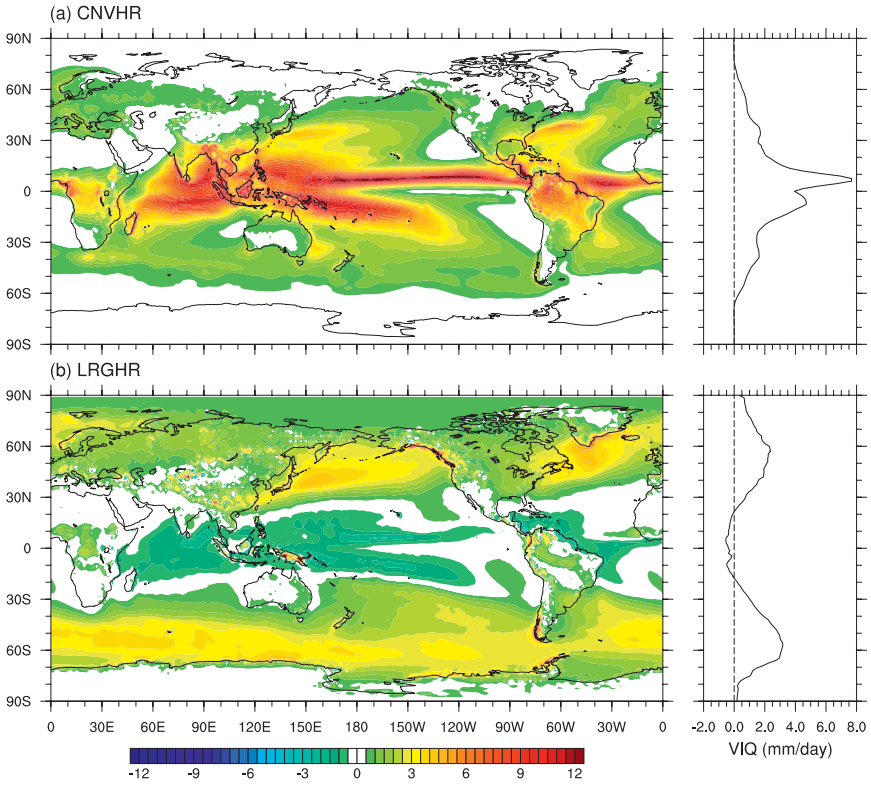

FIG. 6. (left) Time-mean VIQ (mm day^{-1}) and (right) its zonal mean derived from the component of (a) convection heating and (b) large-scale condensation of CFSR.

The CFSR direct heating output includes different components of diabatic heating to allow an exploration of possible dominant components at a given certain latitude. Time and zonal means of VIQ for the convection and the large-scale condensation from CFSR are displayed in Fig. 6. It shows that latent heating in the tropics is exclusively from convective processes. Heating due to large-scale condensation dominates in the extratropics, with its peak at about 60° latitude in each hemisphere. Heating from convection and large-scale condensation is equal at about 40° latitude in both hemispheres. It is unknown to what extent this variation in convective and large-scale heating with latitude is realistic or an artificial product of the data assimilation model.

c. *Dependence on rain rates*

The dependence of heating profiles on rain rates (approximated by VIQ), which has been examined at the sounding locations (Fig. 4), can be expanded to the global tropics and extratropics. Over the tropical oceans (20°S–20°N), the levels of primary heating peaks (marked by dotted lines) in the three reanalyses are different (Fig. 7, left). Heating peaks of CFSR Q1 and QT (Figs. 7c,g) are the lowest, at 700 hPa for all precipitation rates (except the extremes >25 mm day^{-1}, which are very rare). In ERA-Interim Q1 (Fig. 7a) and MERRA Q1 and QT (Figs. 7e,i), heating peaks are at a slightly higher level (550–600 hPa) for rain rates up to 18–22 mm day^{-1} and then jump to the upper troposphere (350–450 hPa) for larger rain rates. Over tropical land (Fig. 7, right), heating peaks are systematically higher than over the tropical oceans in CFSR and MERRA (at most rain rates) but not in ERA-Interim.

Both ERA-Interim and MERRA show unambiguous double peak structures over the tropical oceans at most rain rates. However, the peak levels are quite different. Over tropical land, the double peak structure almost disappears in ERA-Interim (Fig. 7b) but remains in MERRA (Figs. 7f,j) for light rain (<10 mm day^{-1}). This suggests that the vertical structure of the heating profiles in the reanalyses and their differences must be understood as a consequence of interaction between model cumulus parameterization and the large-scale environment. This notion will be repeated in the rest of the study.

The vertical structure of Q1 agrees with QT in general. However, the double peak structure of MERRA seems to be more obvious in QT, especially over land. Cooling above the boundary layer at negative VIQ is much stronger in QT than Q1 in CFSR. A gradual

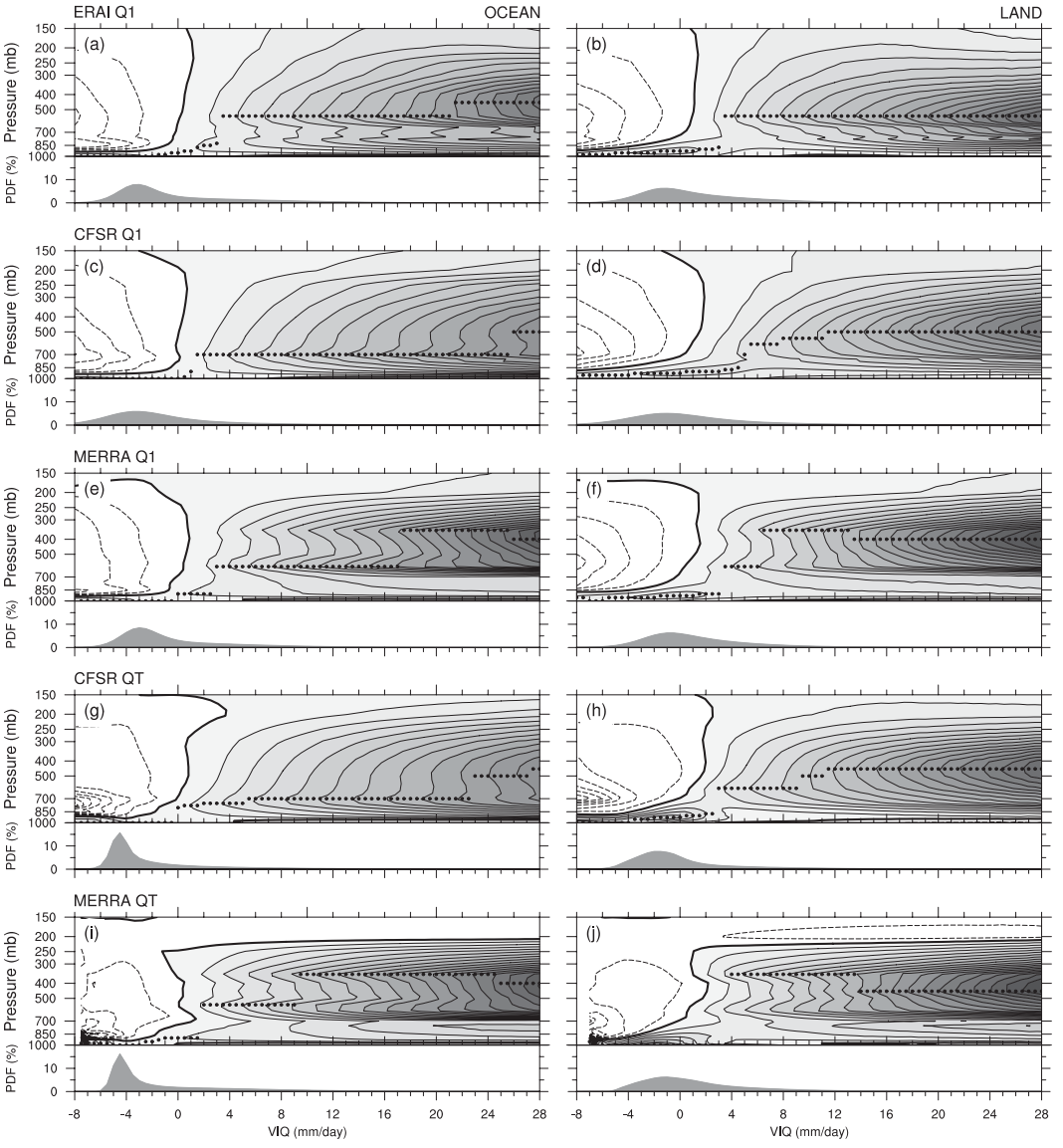

FIG. 7. Diabatic heating profiles (interval of 1 K day^{-1}) as functions of (top) VIQ and (bottom) PDFs of VIQ from (a),(b) ERA-Interim Q1; (c),(d) CFSR Q1; (e),(f) MERRA Q1; (g),(h) CFSR QT; and (i),(j) MERRA QT over (left) the oceans and (right) land between 20°S and 20°N. The VIQ bin width is 0.5 mm day^{-1}. The primary peak of each bin is marked by a black dot. Dashed contours are for negative values, bold contours are for zeros, and positive values are highlighted by shading.

increase in the altitude of the heating peak with increasing rain rates can be discerned only in CFSR QT over the ocean and CFSR Q1 and QT over land. The PDF of VIQ is narrower for QT than Q1 for both CFSR and MERRA. The differences between Q1 and QT will be further discussed in section 4 with their speculative explanations.

The double peak structures in the heating profiles seen in the tropics disappear over the Northern Hemispheric oceans outside the tropics (40°–60°N) in MERRA and become very weak in ERA-Interim and CFSR Q1 (Fig. 8). Similar results are found over ocean and in the Southern Hemisphere (not shown). It appears that diabatic heating profiles from the three reanalyses agree with each other more at midlatitudes than in the tropics. Diabatic heating at midlatitudes is mainly produced by large-scale condensation, whereas it is produced mainly by cumulus parameterization in the tropics (Fig. 6). This points to cumulus parameterization as the main suspect for the disagreement among the reanalyses. However, as we repeatedly demonstrate, cumulus parameterization alone cannot explain all the disagreement.

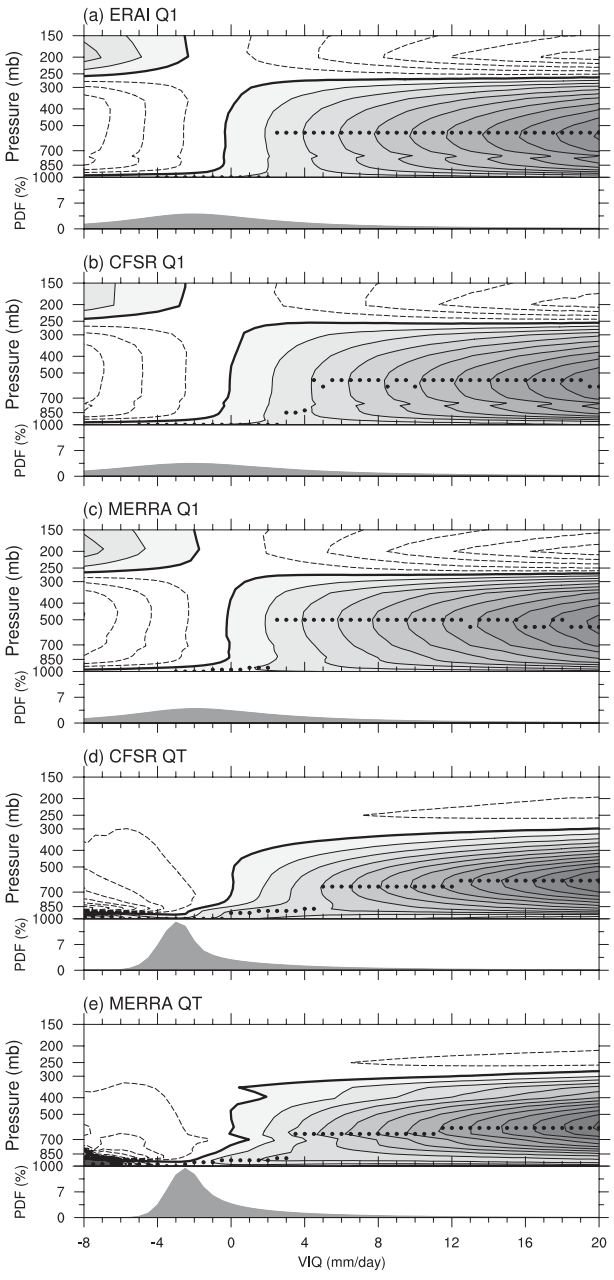

FIG. 8. As in Fig. 7, but over the oceans between 40° and 60°N.

d. ITCZ

Time- and zonal-mean diabatic heating profiles in the ITCZ have been seen in Fig. 5. However, heating profiles are very different among the ITCZs over different oceans and in different seasons. More detailed characteristics of diabatic heating profiles in the ITCZ are explored in this subsection.

Vertical structures of diabatic heating in the ITCZs over the Indian Ocean (60°–90°E), eastern Pacific Ocean (90°–120°W), and Atlantic Ocean (20°–40°W) during their peak months are shown in Fig. 9. Their similarities and differences among the reanalyses and among the ocean basins are obvious. In all three reanalyses, the Indian Ocean ITCZ (Fig. 9, left) is the widest in latitude, presumably related to the equatorial warm pool and a lack of a cold tongue there. Heating profiles are more vertically confined in the Atlantic ITCZ (Fig. 9, right) than in the other two ITCZs in MERRA and ERA-Interim. The vertical confinement in the heating profiles of MERRA in the Atlantic ITCZ comes from the weakening or disappearance of the strong upper-level peak (400–300 hPa) seen in the Indian Ocean and eastern Pacific ITCZs. Possible explanations for this vertical confinement of the Atlantic ITCZ, if real, include lower SST at the general latitude of the Atlantic ITCZ during its peak season and effects of dry air coming out of Africa (Zhang and Pennington 2004). However, it is puzzling why the Atlantic ITCZ heating profile in CFSR is immune of this confinement.

There is a poleward tilt in the heating profiles in all three reanalyses over the eastern Pacific ITCZ, which is absent in the Atlantic ITCZ. Heating profiles in the Indian Ocean ITCZ appear to tilt equatorward in the lowest part of the atmosphere. Outside the ITCZs, boundary layer heating in the winter hemisphere exists over the Atlantic Ocean and eastern Pacific but not over the Indian Ocean in all reanalyses. Also in the winter hemisphere, there is a shallow cooling layer immediately above the boundary layer in almost all heating products. These vertical heating and cooling couplet is presumably a signal of latent heating and radiative cooling of marine stratus clouds (Nigam 1997). The depth and strength of the heating–cooling couplet vary in location and among the reanalyses.

The most evident disagreement among the reanalyses is the number and level of heating peaks seen previously. The multipeak structure is the most prominent in MERRA, with three peaks in its QT in all three ITCZs (Figs. 9m–o). ERA-Interim produces double peaks in the eastern Pacific and Atlantic ITCZs (Figs. 9b,c). CFSR produces double peaks only in Q1 of the eastern Pacific ITCZ (Fig. 9e).

Double ITCZs occur in different seasons over different oceans (Zhang 2001). Their vertical heating profiles during selected months are shown in Fig. 10. The three reanalyses consistently demonstrate very shallow heating (below the 500-hPa level) in the classic double ITCZs over the eastern Pacific (90°–120°W) that usually occurs in March–April (Fig. 10, right). This is a sharp contract to the deep heating in the summer there (Fig. 9, middle). Low-level cooling above the boundary layer on the polar sides is stronger in the Southern Hemisphere than in the Northern Hemisphere.

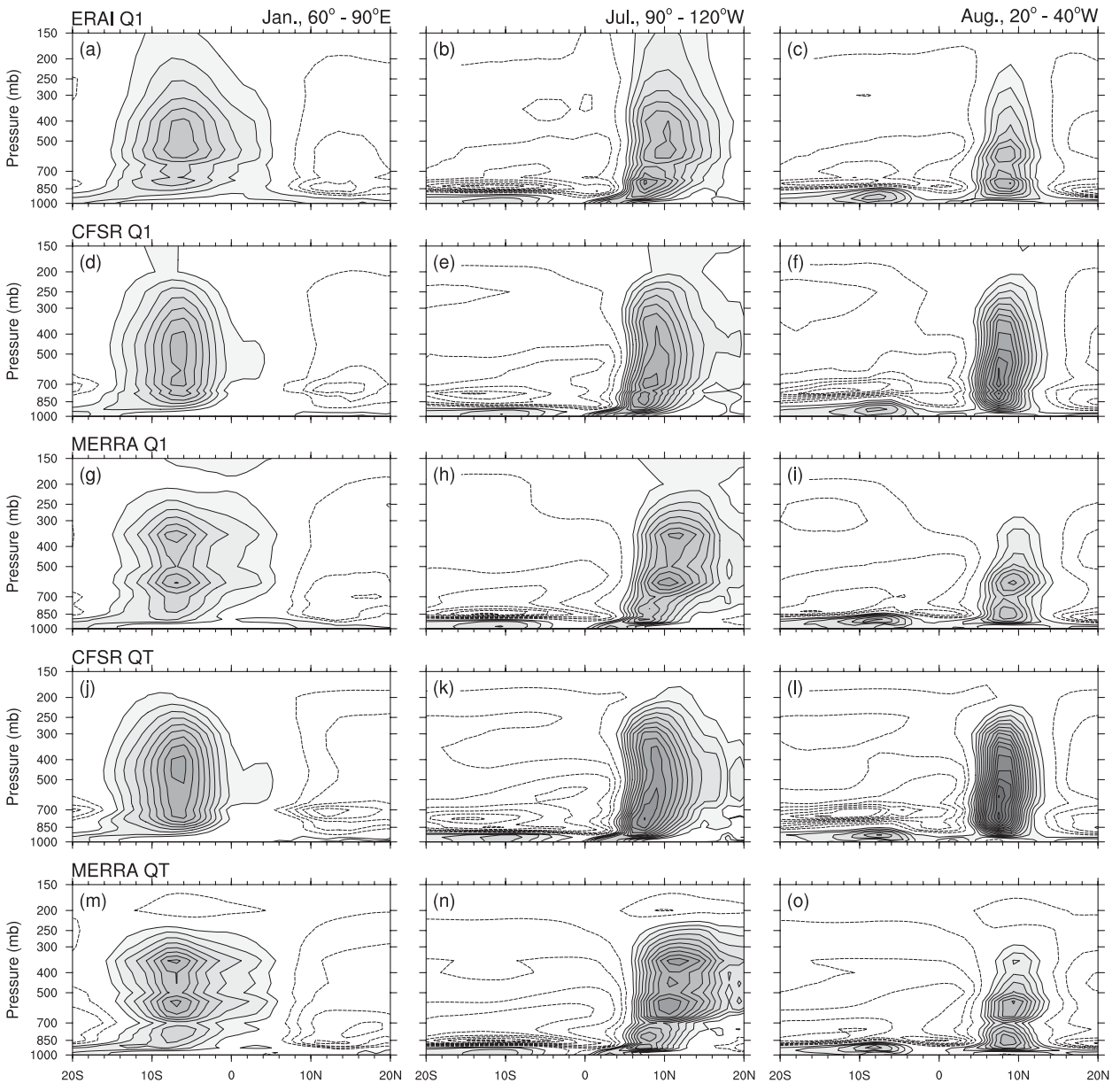

FIG. 9. Time-mean diabatic heating (interval of 0.5 K day^{-1}) averaged over (left) the Indian Ocean (60°–90°E) in January, (middle) the eastern Pacific Ocean (90°–120°W) in July, and (right) the Atlantic Ocean (20°–40°W) in August from (a)–(c) ERA-Interim Q1, (d)–(f) CFSR Q1, (g)–(i) MERRA Q1, (j)–(l) CFSR QT, and (m)–(o) MERRA QT. Dashed contours are for negative values, zero contours are omitted, and positive values are highlighted by shading.

Double ITCZs over the western and central Pacific (150°E–180°) are actually a combination of the ITCZ north of the equator and part of the SPCZ south of the equator. However, they share the same meridional characteristics with the conventional double ITCZs: namely, a heating minimum at the equator flanked by heating maxima on both sides (Fig. 10, middle). As seen in the single ITCZs, the reanalyses produce very different vertical structures of diabatic heating in the double ITCZs over the western and central Pacific. The double peak structure is the most obvious in MERRA (Figs. 10h,n), much less so in ERA-Interim (Fig. 10b), and absent in CFSR Q1 and QT (Figs. 10e,k).

Over the Indian Ocean (60°–90°E; Fig. 10, left), double ITCZs are in general less distinct than over the other two oceans, possibly because of the lack of a cold tongue there. However, this suggests that a double ITCZ can exist over a uniform warm pool. It is discernible, even

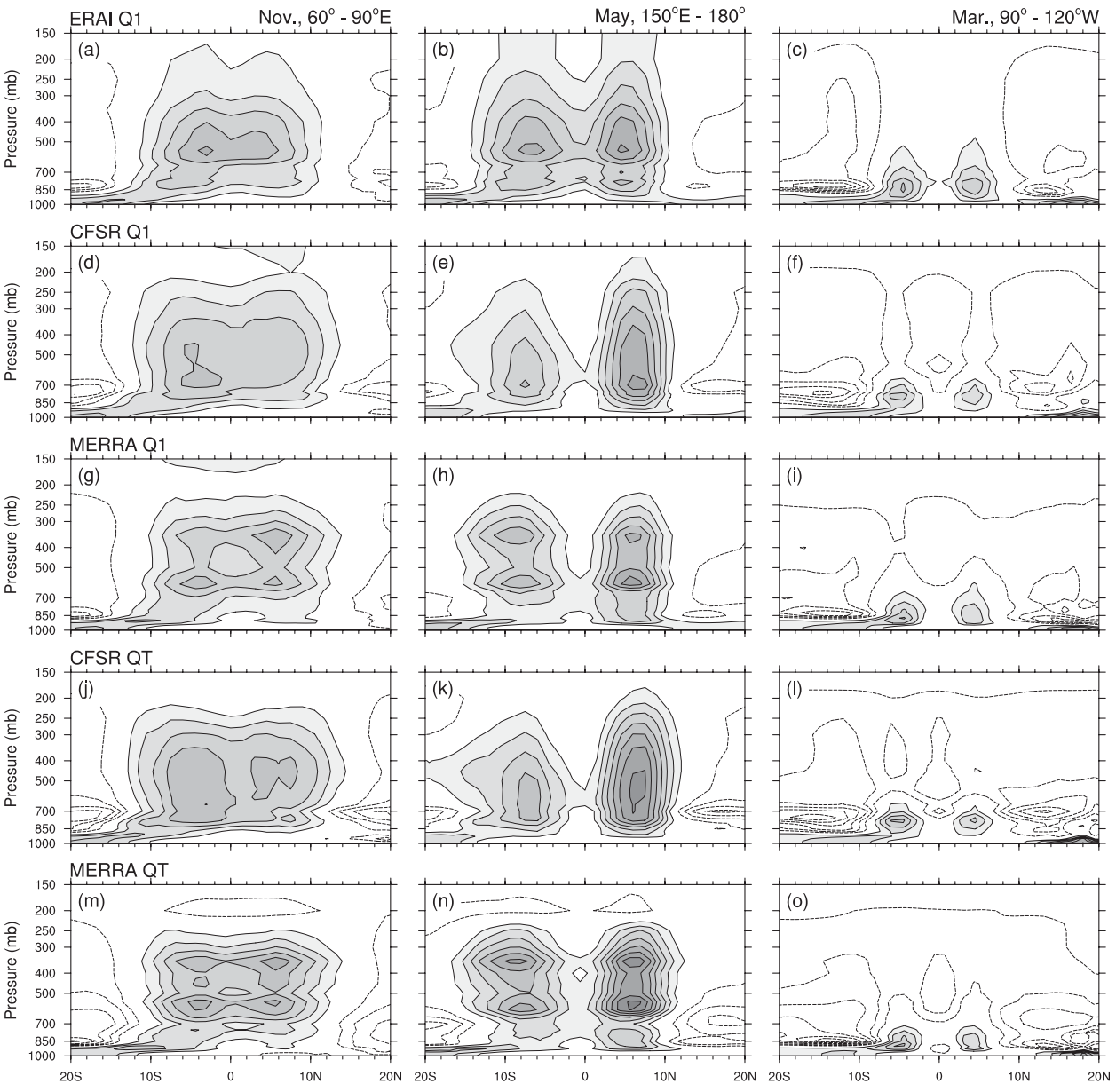

FIG. 10. Time-mean diabatic heating (interval of 0.5 K day^{-1}) averaged over (left) the Indian Ocean (60°–90°E) in November, (middle) the western and central Pacific (150°E–180°) in May, and (right) the eastern Pacific (90°–120°W) in March from (a)–(c) ERA-Interim Q1, (d)–(f) CFSR Q1, (g)–(i) MERRA Q1, (j)–(l) CFSR QT, and (m)–(o) MERRA QT. Dashed contours are for negative values, zero contours are omitted, and positive values are highlighted by shading.

though not completely separated, in MERRA and CFSR QT but not in ERA-Interim and CFSR Q1. The discrepancies in single versus double heating peaks among the reanalyses also exist over the Indian Ocean.

If there are similarities and disagreement among the reanalyses in their heating profiles in the single and double ITCZs, the disagreement is more profound in their seasonal cycle, as seen in Fig. 11. This figure is generated by first identifying the latitude of the ITCZ center (maximum VIQ) in each month, which migrates meridionally with time, and then plotting the mean vertical profiles of diabatic heating at that latitude for each month averaged over the same longitudes as in Figs. 9 and 10. The figure depicts the seasonal evolution (twice for better visual effects) in vertical structures of diabatic heating following the seasonal migrations of the ITCZs in a Lagrangian sense. The Indian Ocean ITCZ (Fig. 11, left) is south of the equator, while the other two are north of the equator.

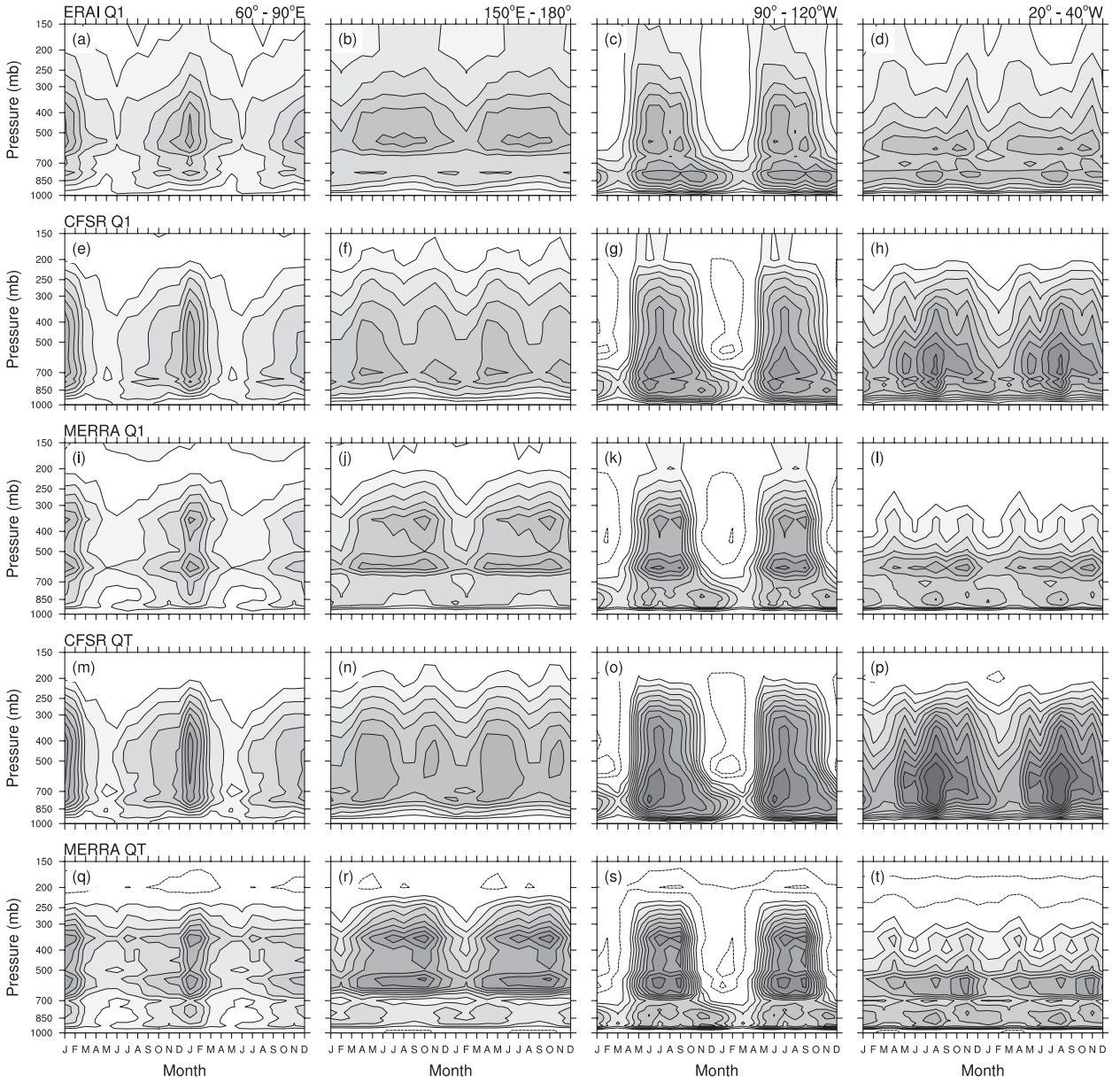

FIG. 11. Lagrangian double seasonal cycles of ITCZ heating profiles from (a)–(d) ERA-Interim Q1, (e)–(h) CFSR Q1, (i)–(l) MERRA Q1, (m)–(p) CFSR QT, and (q)–(t) MERRA QT (interval of 0.5 K day^{-1}) zonally averaged over (left)–(right) the Indian Ocean (60°–90°E), the western and central Pacific (150°E–180°), the eastern Pacific Ocean (90°–120°W), and the Atlantic Ocean (20°–40°W) following the latitudes of the ITCZ centers (maximum VIQ) in each month. Dashed contours are for negative values, zero contours are omitted, and positive values are highlighted by shading.

Heating of the Indian Ocean ITCZ reaches its maximum in January–February in all reanalyses (Fig. 11, left). There is a slight time asymmetry with a gradual build-up toward the January–February heating maximum and an abrupt reduction after that. Again, MERRA Q1 and QT exhibit unambiguously a double peak structure, with a third peak in MERRA QT at 800 hPa. ERA-Interim produces the primary heat peak at 550 hPa with a very weak secondary peak at 800 hPa. CFSR produces a single peak deep heating profile.

The seasonal evolution in the heating profile of the western–central Pacific Ocean ITCZ or the northern branch of the double ITCZ there (second column from the left in Fig. 11) is very different from that of the Indian Ocean ITCZ. The western–central Pacific ITCZ is persistently strong throughout the entire year, except

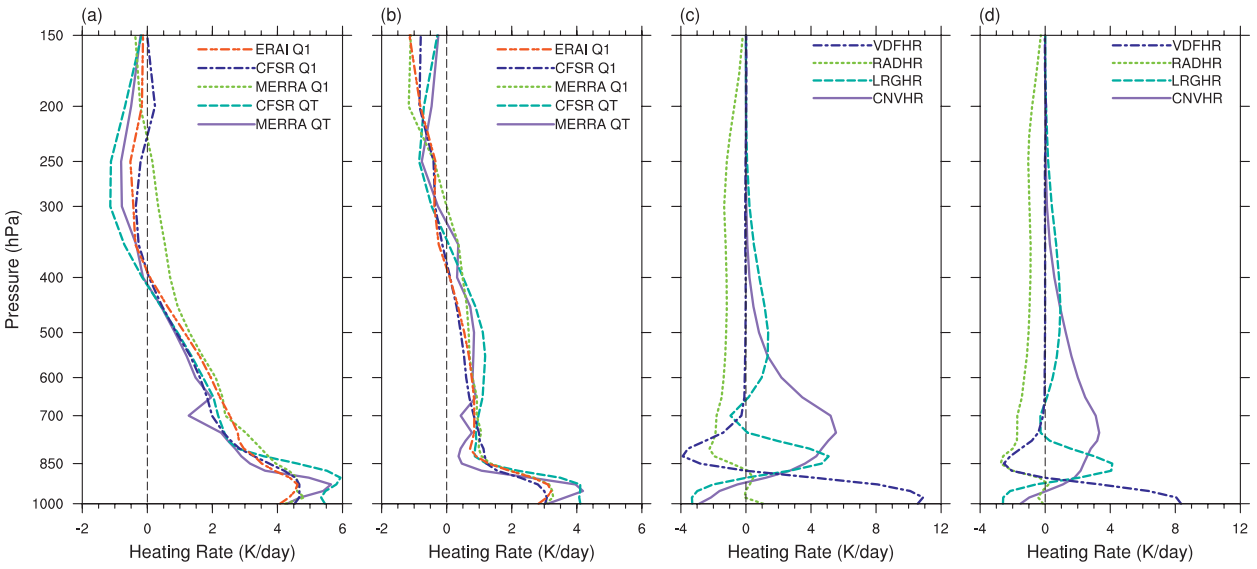

FIG. 12. January-mean diabatic heating profiles from the reanalyses in the storm tracks over (a) the northern Pacific Ocean (30°–40°N, 145°–165°E) and (b) the northern Atlantic Ocean (30°–40°N, 50°–70°W). (c),(d) As in (a),(b), but for heating components of vertical diffusion (VDFHR), convection (CNVHR), large-scale condensation (LRGHR), and radiation (RADHR) from CFSR.

during January and February, in ERA-Interim and MERRA. CFSR, however, produces a unique semiannual cycle in its Q1 and QT, with the primary peak in April–May and a secondary peak in November. MERRA again produces clearly two peaks in Q1 and three in QT.

The seasonal cycle of the eastern Pacific ITCZ demonstrates yet another different characteristic (second column from the right in Fig. 11) in all reanalyses. The sharp contrast between deep heating during boreal summer and shallow heating in boreal spring could be easily misinterpreted as an ITCZ comes and goes. In fact, it is a transformation between the single, deep ITCZ in summer (Fig. 9, middle) and shallow double ITCZs in spring (Fig. 10, right). The transition between the shallow to deep heating in April and October is very rapid. If the rapid transition in April can be explained by the fast increase in the underneath SST, then that in October needs a different explanation, because SST decrease gradually at that time (de Szoeke and Xie 2008). Low-level (below the 700-hPa level) heating is much stronger over the eastern Pacific than the other oceans. This shallow heating exists not only during the double ITCZ season but also in the months when ITCZ heating is deep. With this shallow heating, MERRA Q1 and QT shows three peaks and ERA-Interim produces evident two peaks in their heating profiles. Implications of the shallow versus deep heating in the eastern Pacific ITCZ will be discussed in section 4.

Seasonal evolutions and vertical structures of diabatic heating in the Atlantic ITCZ (Fig. 11, right) are still different from those in the other ITCZs, and the reanalyses differ substantially from each other. All three reanalyses produce relatively weak tropospheric heating in February and peculiar subseasonal variability in mid–upper-tropospheric heating. Heating profiles of ERA-Interim and MERRA Q1 share some similarities. They both have two peaks. MERRA Q1 in the Atlantic ITCZ is the shallowest (capped at 300 hPa) among all. Diabatic heating of CFSR is much deeper.

The astonishing disagreement in the vertical structures and their seasonal evolutions in the different ITCZs and among the different reanalyses post a great challenge to their explanations and applications. Further discussions on this will be given in section 4.

e. Storm track

Diabatic heating in the Northern Hemispheric storm tracks reach its maximum in January over both the Pacific and Atlantic Oceans. Its mean vertical structure exhibits maximum within the boundary layer in all reanalyses (Figs. 12a,b), due to surface sensible heat flux. Above the boundary layer, total diabatic heating is a combination of heating due to convective processes and large-scale condensation as shown in Fig. 6. It is mainly confined to the lower troposphere (below the 400-hPa level). All reanalyses appear to agree with each other here better than in the tropics. The CFSR output of individual heating components (Figs. 12c,d) indicate that convective heating is shallower than heating because of large-scale condensation, and radiative cooling peaks at the same level of heating peak of large-scale condensation (850 hPa). These results are interesting but cannot be cross-validated

or compared because these individual heating components are not available from ERA-Interim and MERRA.

4. Summary and discussion

Vertical structures of diabatic heating from three most recent global reanalyses (ERA-Interim, CFSR, and MERRA) have been evaluated against sounding observations and compared with each other. The main objective of the evaluation and comparison is to assess the degree to which diabatic heating profiles produced by the reanalyses can be reliably used in place of those based on sounding observations. Both Q1 (estimated total diabatic heating as a residual of the heat budget using wind and temperature data) and QT (direct output of temperature tendency due to diabatic processes) from the reanalyses were included. The main results are as follows:

(i) Vertical structures of diabatic heating produced by the reanalyses match well those based on the sounding observations at some locations but not at others (Fig. 2). In general, heating profiles produced by the reanalyses and those based on the sounding observations agree better at larger rain rates (approximated by VIQ) and better over the open ocean than over land or coastal regions. Agreement among the reanalysis products does not necessarily suggest their realism. The limited sounding observations are insufficient for a global evaluation of diabatic heating profiles produced by the reanalyses.

(i) Diabatic heating profiles produced by the reanalyses agree with each other in their gross features, such as the distinct vertical structures in the single versus double ITCZs (Figs. 9, 10), the distinct seasonal cycles in the ITCZs over different ocean basins (Fig. 11), and the contrast between tropics and extratropics (Fig. 5). They agree with each other better in the extratropics (e.g., storm tracks) than in the tropics.

(iii) There are evident, severe disagreements among the three reanalyses in their tropical diabatic heating profiles. MERRA tends to produce multiple heating peaks, sometimes three: one in the boundary layer, one in the lower troposphere, and one in the upper troposphere. ERA-Interim tends to produce two peaks, while CFSR usually produces only one peak in the lower troposphere.

(iv) Q1 is in general an adequate proxy of QT, even though it may underestimate the amplitude of QT, it may overestimate the cooling in the upper troposphere in the extratropics, and its vertical profiles are smoother than QT. The main agreement and disagreement in vertical structures of diabatic heating between the reanalyses and sounding observations and between different reanalyses are well captured by Q1.

The general agreement between Q1 and QT indicates the consistency between the large-scale environment (wind and temperature) as input to cumulus parameterization that produces QT and to the thermodynamic equation that is used to calculate Q1. When observations are available to constrain wind and temperature in the reanalyses, they feed to parameterization schemes. In the absence of observations, wind and temperature respond to heating generated by parameterization schemes. The disagreement of the Q1 and QT is mainly caused by the Q1 data sources. QT in the assimilation system is calculated and accumulated on the model levels with higher vertical and horizontal resolution. Q1 was estimated on the fixed pressure level with lower vertical and horizontal resolution. The vertical profiles of Q1 are thus smoother than those of QT. Furthermore, QT in the assimilation system was calculated at each time step, and the time interval is much shorter than that of the Q1 estimates (24 h), which may miss some physical process of short time scales. Discrepancies between Q1 and QT can also come from numerical errors introduced by calculating divergence in the procedure of estimating Q1 (Katsumata et al. 2011).

The disagreement in the diabatic heating profiles among the reanalyses cannot be left without explanations. In the tropics, where most diabatic heating come from parameterized precipitation in the data assimilation models, cumulus parameterization schemes are likely to be the main sources of the disagreement. A testament of this comes from the fact that the three reanalyses agree with each other better in their diabatic heating profiles in the extratropics, where large-scale condensation dominates, than in the tropics, where convective processes dominate (Fig. 6). However, cumulus parameterization cannot be the sole source of the disagreement among the reanalyses. Cloud radiation can contribute to vertical diabatic heating profiles (Mather et al. 2007), and its parameterization can therefore be another source of the disagreement. Within a given reanalysis, diabatic heating can exhibit quite different vertical structures in different part of the tropics (Figs. 9, 11), suggesting influences by the large-scale convective environment. The degree to which the disagreement among the diabatic heating profiles of the three reanalyses comes from their cumulus parameterization versus their other possible sources (other parameterization schemes, data assimilation procedures, etc.) cannot be known from the simple comparisons presented here. It would be interesting to see if the same disagreement in the heating profiles exists in climate simulations by the

same models that produced the reanalyses but without observational constraints (except sea surface temperature).

It is unlikely that the two or three peaks seen in the time-mean heating profiles of the reanalyses (especially MERRA) actually occur simultaneously at a given location and time. It is more reasonable to expect they emerge at the same location but different times. In other words, the two or three peaks in the mean heating profiles may imply two or three types of dominant convective systems, such as shallow, intermediate, and deep convection. On the other hand, a single heating peak (e.g., in CFSR) may suggest a single dominant convective system in a convective continuum with convective systems of all depths. The limited Q1 data based on the sounding observations seem to suggest a convective continuum instead of multiple discrete dominant convective types (Fig. 4d). However, previous observational diagnostics have suggested tropical trimodal convective clouds (Johnson et al. 1999) and bimodal heating (Zhang and Hagos 2009). These discrepancies among observations need to be reconciled by further analysis and perhaps using new in situ data.

The different number of heating peaks and their levels in the ITCZs produced by the three reanalyses may have implications to their meridional-vertical circulations. In addition to the classic, Hadley-type deep meridional circulation, shallow meridional circulations with its upper-level return flow in the lower to mid troposphere have been observed over the eastern Pacific (Zhang et al. 2004), West Africa (Zhang et al. 2006), and other equatorial regions (Zhang et al. 2008). Such shallow meridional circulations exist when deep convection in the ITCZ is absent (Nolan et al. 2010). It is possible but yet to be shown that the different vertical structures of diabatic heating produced by the three reanalyses may imply different vertical structures of their meridional circulations. If so, their application may lead to different conclusions. For example, a trajectory analysis may yield different patterns of aerosol transport and mixture over West Africa and the tropical Atlantic Ocean, where the segregation and mixing of Saharan dust north of the ITCZ and biomass burning smoke south of it depend on the vertical structures of the meridional circulation.

Comparisons for heating profiles in the Southern Hemispheric convergence zones in the Pacific, Atlantic, and Indian Oceans (i.e., those that extend southeastward instead of elongate zonally) led to results (not shown) similar to those for the ITCZs. Diabatic heating in the monsoon regions are not presented in this study for the following reason. There are large discrepancies among the reanalyses in their rainfall (VIQ) distributions and intensity over land. Comparisons of vertical structures of monsoon diabatic heating are therefore not straightforward. They should not be done at fixed locations and time. A meaningful comparison of monsoon heating profiles from the reanalyses should follow the migration of monsoon rainfall through a monsoon season. This needs to be treated properly in a separated study.

Temporal fluctuations in diabatic heating profiles associated with the rich variety of tropical perturbations are not included in this study. A westward tilt of diabatic heating associated with the MJO (Lin et al. 2004) has been explored using heating data from different reanalyses and satellite retrievals (Zhang et al. 2010; Ling and Zhang 2011; Jiang et al. 2011) with inconsistent results. Observations have shown transitions from shallow convection to midlevel congestus then to deep convection in the tropics (Johnson et al. 1999; Kikuchi and Takayabu 2004). This gradual increase in latent heating levels appears to happen on different scales and hence a cross-scale ''self-similarity'' in vertical structures of convective systems (Mapes et al. 2006; Kiladis et al. 2009). It is unclear if this self-similarity is reproduced by any of the reanalyses.

The results from this study indicate that diabatic heating from the three reanalyses, either Q1 or QT, is useful to describe its gross features (e.g., meridional distributions in the zonal means, general contrast between the ITCZs in the different oceans). However, vertical structures of their diabatic heating in the tropics suffer from substantial disagreement among themselves and large biases in comparison to sounding observations, even when their disagreement is minimal. Cautions, therefore, must be exercised when diabatic heating profiles from the reanalyses are used in either diagnostics for better understanding or validation of numerical model simulations. Currently, the only way to obtain reliable diabatic heating profiles is through sounding observations. For a global evaluation of vertical structures of diabatic heating produced by data assimilation products (reanalyses) and numerical models, the currently available observational sample size is inadequate and must be increased. Sounding data from past field campaigns in the predigital era are being rescued (Johnson et al. 2012). Future tropical field campaigns deploying sounding arrays that allow estimated diabatic heating profiles must continue. Such sounding observations would be particularly beneficial if paired with radar observations that provide detailed information of clouds. The issue of diabatic heating profiles, especially the level and number of their peaks, needs to be addressed with knowledge of the population and structure of clouds that produce the heating profiles.

Acknowledgments. The authors thank Peter Bechtold for comments on ERA-Interim assimilation systems. Courtney Schumacher and two anonymous reviewers

provided constructive comments on an early manuscript of this study. The availability of the reanalysis data from ERA-Interim, CFSR, and MERRA, especially the direct output of QT from CFSR and MERRA, are highly appreciated. Richard Johnson and Paul Ciesielski made most of the sounding Q1 calculations. This study was supported by a grant by NOAA's Modeling, Analysis, Prediction and Projection (MAPP) program.

REFERENCES

Chan, S. C., and S. Nigam, 2009: Residual diagnosis of diabatic heating from ERA-40 and NCEP reanalyses: Intercomparisons with TRMM. *J. Climate,* **22,** 414–428.

Cho, H. R., and D. Pendlebury, 1997: Wave CISK of equatorial waves and the vertical distribution of cumulus heating. *J. Atmos. Sci.,* **54,** 2429–2440.

Dee, D. P., and Coauthors, 2011: The ERA-Interim reanalysis: Configuration and performance of the data assimilation system. *Quart. J. Roy. Meteor. Soc.,* **137,** 553–597.

de Szoeke, S. P., and S.-P. Xie, 2008: The tropical eastern Pacific seasonal cycle: Assessment of errors and mechanisms in IPCC AR4 coupled ocean–atmosphere general circulation models. *J. Climate,* **21,** 2573–2590.

Ding, Y. H., C. Y. Li, and Y. J. Liu, 2004: Overview of the South China Sea Monsoon Experiment. *Adv. Atmos. Sci.,* **21,** 343–360.

Hagos, S., and Coauthors, 2010: Estimates of tropical diabatic heating profiles: Commonalities and uncertainties. *J. Climate,* **23,** 542–558.

Hartmann, D. L., H. H. Hendon, and R. A. Houze, 1984: Some implications of the mesoscale circulations in tropical cloud clusters for large-scale dynamics and climate. *J. Atmos. Sci.,* **41,** 113–121.

Higgins, W., and Coauthors, 2006: The NAME 2004 field campaign and modeling strategy. *Bull. Amer. Meteor. Soc.,* **87,** 79.

Hirota, N., Y. N. Takayabu, M. Watanabe, and M. Kimoto, 2011: Precipitation reproducibility over tropical oceans and its relationship to the double ITCZ problem in CMIP3 and MIROC5 climate models. *J. Climate,* **24,** 4859–4873.

Houze, R. A., 1997: Stratiform precipitation in regions of convection: A meteorological paradox? *Bull. Amer. Meteor. Soc.,* **78,** 2179–2196.

Huffman, G. J., and Coauthors, 2007: The TRMM Multisatellite Precipitation Analysis (TMPA): Quasi-global, multiyear, combined-sensor precipitation estimates at fine scales. *J. Hydrometeor.,* **8,** 38–55.

Jiang, X., and Coauthors, 2011: Vertical diabatic heating structure of the MJO: Intercomparison between recent reanalyses and TRMM estimates. *Mon. Wea. Rev.,* **139,** 3208–3223.

Johnson, R. H., T. M. Rickenbach, S. A. Rutledge, P. E. Ciesielski, and W. H. Schubert, 1999: Trimodal characteristics of tropical convection. *J. Climate,* **12,** 2397–2418.

——, S. F. Williams, and P. E. Ciesielski, 2012: Legacy Atmospheric Sounding Dataset project. *Bull. Amer. Meteor. Soc.,* **93,** 14–17.

Katsumata, M., P. E. Ciesielski, and R. H. Johnson, 2011: Evaluation of budget analyses during MISMO. *J. Appl. Meteor. Climatol.,* **50,** 241–254.

Kikuchi, K., and Y. N. Takayabu, 2004: The development of organized convection associated with the MJO during TOGA COARE IOP: Trimodal characteristics. *Geophys. Res. Lett.,* **31,** L10101, doi:10.1029/2004GL019601.

Kiladis, G. N., M. C. Wheeler, P. T. Haertel, K. H. Straub, and P. E. Roundy, 2009: Convectively coupled equatorial waves. *Rev. Geophys.,* **47,** RG2003, doi:10.1029/2008RG000266.

Kummerow, C., and Coauthors, 2000: The status of the Tropical Rainfall Measuring Mission (TRMM) after two years in orbit. *J. Appl. Meteor.,* **39,** 1965–1982.

L'Ecuyer, T. S., and G. L. Stephens, 2003: The tropical oceanic energy budget from the TRMM perspective. Part I: Algorithm and uncertainties. *J. Climate,* **16,** 1967–1985.

Li, C. Y., X. L. Jia, J. Ling, W. Zhou, and C. D. Zhang, 2009: Sensitivity of MJO simulations to diabatic heating profiles. *Climate Dyn.,* **32,** 167–187.

Lin, J. L., B. Mapes, M. H. Zhang, and M. Newman, 2004: Stratiform precipitation, vertical heating profiles, and the Madden–Julian oscillation. *J. Atmos. Sci.,* **61,** 296–309.

Lin, X., and R. H. Johnson, 1996: Heating, moistening, and rainfall over the western Pacific warm pool during TOGA COARE. *J. Atmos. Sci.,* **53,** 3367–3383.

Ling, J., and C. D. Zhang, 2011: Structural evolution in heating profiles of the MJO in global reanalyses and TRMM retrievals. *J. Climate,* **24,** 825–842.

Madden, R. A., and P. R. Julian, 1971: Detection of a 40–50 day oscillation in zonal wind in the tropical Pacific. *J. Atmos. Sci.,* **28,** 702–708.

——, and ——, 1972: Description of global-scale circulation cells in tropics with a 40–50 day period. *J. Atmos. Sci.,* **29,** 1109–1123.

Mapes, B. E., 2000: Convective inhibition, subgrid-scale triggering energy, and stratiform instability in a toy tropical wave model. *J. Atmos. Sci.,* **57,** 1515–1535.

——, and R. A. Houze Jr., 1995: Diabatic divergence profiles in western Pacific mesoscale convective systems. *J. Atmos. Sci.,* **52,** 1807–1828.

——, S. Tulich, J. Lin, and P. Zuidema, 2006: The mesoscale convection life cycle: Building block or prototype for large-scale tropical waves? *Dyn. Atmos. Oceans,* **42,** 3–29.

Mather, J. H., S. A. McFarlane, M. A. Miller, and K. L. Johnson, 2007: Cloud properties and associated heating rates in the tropical western Pacific. *J. Geophys. Res.,* **112,** D05201, doi:10.1029/2006JD007555.

May, P. T., J. H. Mather, G. Vaughan, C. Jakob, G. M. McFarquhar, K. N. Bower, and G. G. Mace, 2008: The Tropical Warm Pool International Cloud Experiment. *Bull. Amer. Meteor. Soc.,* **89,** 629–645.

Nigam, S., 1997: The annual warm to cold phase transition in the eastern equatorial Pacific: Diagnosis of the role of stratus cloud-top cooling. *J. Climate,* **10,** 2447–2467.

——, C. Chung, and E. DeWeaver, 2000: ENSO diabatic heating in ECMWF and NCEP–NCAR reanalyses, and NCAR CCM3 simulation. *J. Climate,* **13,** 3152–3171.

Nolan, D. S., S. W. Powell, C. Zhang, and B. E. Mapes, 2010: Idealized simulations of the intertropical convergence zone and its multilevel flows. *J. Atmos. Sci.,* **67,** 4028–4053.

Rabier, F., H. Jarvinen, E. Klinker, J. F. Mahfouf, and A. Simmons, 2000: The ECMWF operational implementation of four-dimensional variational assimilation. I: Experimental results with simplified physics. *Quart. J. Roy. Meteor. Soc.,* **126,** 1143–1170.

Rienecker, M. M., and Coauthors, 2011: MERRA: NASA's Modern-Era Retrospective Analysis for Research and Applications. *J. Climate,* **24,** 3624–3648.

Saha, S., and Coauthors, 2010: The NCEP Climate Forecast System Reanalysis. *Bull. Amer. Meteor. Soc.,* **91,** 1015–1057.

Schumacher, C., R. A. Houze, and I. Kraucunas, 2004: The tropical dynamical response to latent heating estimates derived from the TRMM precipitation radar. *J. Atmos. Sci.,* **61,** 1341–1358.

——, P. E. Ciesielski, and M. H. Zhang, 2008: Tropical cloud heating profiles: Analysis from KWAJEX. *Mon. Wea. Rev.,* **136,** 4289–4300.

Shige, S., Y. N. Takayabu, W. K. Tao, and D. E. Johnson, 2004: Spectral retrieval of latent heating profiles from TRMM PR data. Part I: Development of a model-based algorithm. *J. Appl. Meteor.,* **43,** 1095–1113.

Silva Dias, M. A. F., and Coauthors, 2002: Cloud and rain processes in a biosphere-atmosphere interaction context in the Amazon region. *J. Geophys. Res.,* **107,** 8072, doi:10.1029/2001JD000335.

Tao, W.-K., and Coauthors, 2006: Retrieval of latent heating from TRMM measurements. *Bull. Amer. Meteor. Soc.,* **87,** 1555–1572.

Webster, P., and R. Lukas, 1992: TOGA COARE: The Coupled Ocean-Atmosphere Response Experiment. *Bull. Amer. Meteor. Soc.,* **73,** 1377–1416.

Wu, Z. H., 2003: A shallow CISK, deep equilibrium mechanism for the interaction between large-scale convection and large-scale circulations in the tropics. *J. Atmos. Sci.,* **60,** 377–392.

Yanai, M., S. Esbensen, and J. H. Chu, 1973: Determination of bulk properties of tropical cloud clusters from large-scale heat and moisture budgets. *J. Atmos. Sci.,* **30,** 611–627.

Yoneyama, K., and Coauthors, 2008: Mismo field experiment in the equatorial Indian Ocean. *Bull. Amer. Meteor. Soc.,* **89,** 1889–1903.

Yuter, S. E., R. A. Houze, E. A. Smith, T. T. Wilheit, and E. Zipser, 2005: Physical characterization of tropical oceanic convection observed in KWAJEX. *J. Appl. Meteor.,* **44,** 385–415.

Zhang, C., 2001: Double ITCZs. *J. Geophys. Res.,* **106,** 11 785–11 792.

——, and J. Pennington, 2004: African dry air outbreaks. *J. Geophys. Res.,* **109,** D20108, doi:10.1029/2003JD003978.

——, and S. M. Hagos, 2009: Bi-modal structure and variability of large-scale diabatic heating in the tropics. *J. Atmos. Sci.,* **66,** 3621–3640.

——, M. McGauley, and N. A. Bond, 2004: Shallow meridional circulation in the tropical eastern Pacific. *J. Climate,* **17,** 133–139.

——, P. Woodworth, and G. Gu, 2006: The seasonal cycle in the lower troposphere over West Africa from sounding observations. *Quart. J. Roy. Meteor. Soc.,* **132,** 2559–2582.

——, D. S. Nolan, C. D. Thorncroft, and H. Nguyen, 2008: Shallow meridional circulations in the tropical atmosphere. *J. Climate,* **21,** 3453–3470.

——, and Coauthors, 2010: MJO signals in latent heating: Results from TRMM retrievals. *J. Atmos. Sci.,* **67,** 3488–3508.

Zhang, M., and J. Lin, 1997: Constrained variational analysis of sounding data based on column-integrated budgets of mass, heat, moisture, and momentum: Approach and application to ARM measurements. *J. Atmos. Sci.,* **54,** 1503–1524.

Zhou, W., and J. C. L. Chan, 2005: Intraseasonal oscillations and the South China Sea summer monsoon onset. *Int. J. Climatol.,* **25,** 1585–1609.